Bidirectional Impact of miR-29a modulation on Memory Stability in the Adult Brain

Aurelia Viglione[1,2], Chiara Giannuzzi[1], Elena Putignano[3], Raffaele Mazziotti[3,4,5], Alessandro Cellerino[1,6] and Tommaso Pizzorusso[1,3*]

[1] *BIO@SNS lab, Scuola Normale Superiore, Pisa, Italy;*

[2] *Center for Behavioral Sciences and Mental Health, Istituto Superiore di Sanità, Rome, Italy;*

[3] *Institute of Neuroscience, National Research Council, Pisa, Italy;*

[4] *Department of Developmental Neuroscience, IRCCS Stella Maris Foundation, Pisa, Italy;*

[5] *Department of Neuroscience, Psychology, Pharmacology, and Child Health, University of Florence, Florence, Italy;*

[6] *Leibniz Institute on Aging – Fritz Lipmann Institute (FLI) Jena Germany*

** Corresponding author: Tommaso Pizzorusso, Istituto Neuroscienze CNR and BIO@SNS lab, Scuola Normale Superiore via G. Moruzzi 1, 56124 Pisa, Italy, tel +390503153167, Fax +390503153220, e-mail: tommaso.pizzorusso@sns.it*

Summary

MicroRNAs are key regulators of brain gene expression, with miR-29a notably upregulated from development to adulthood and in aging, and showing links to cognitive decline. However, the extent to which miR-29 levels influence learning and memory processes, and its molecular mediators, remains to be determined. Here, we down- and up-regulated miR-29a levels in the dorsal hippocampus of adult mice to reveal miR-29 role in memory. Inhibiting miR-29a enhanced trace fear memory stability, increased Dnmt3a levels, and affected CpG methylation in gene regulation regions. In contrast, increasing miR-29a impaired memory performances and decreased Dnmt3a levels, suggesting a destabilization of memory processes. Proteomic and transcriptomic analysis demonstrated that miR-29a antagonism upregulated RNA-binding and synaptic proteins and downregulated inflammation and myelin associated proteins. These results underscore miR-29a's pivotal role in memory persistence, plasticity, and cognitive aging, suggesting that miR-29a modulation could offer potential strategies for cognitive enhancement and age-related memory decline.

Keywords

fear conditioning, epigenetics, non-coding RNA, microRNA, hippocampus, neural plasticity, cognitive decline, aging

Introduction

MicroRNAs (miRNAs) are small non-coding RNA molecules that modulate gene expression by binding to complementary sequences in target mRNAs, leading to the repression of translation and transcript destabilization [1]. A single microRNA can bind thousand potential targets fine-tuning gene expression patterns. This feature makes them well-suited for the dynamic and reversible control of gene expression, which is essential for processes like memory formation and maintenance [2,3]. One particular miRNA family, miR-29, has emerged as a potential regulator at the intersection of aging and memory. MiR-29 is extensively involved in various aging-related biological processes, such as apoptosis [4], metabolism [5], neuronal maturation [4], immunity [6,7], and the aging-associated accumulation of iron in the brain [4,8]. Intriguingly, the miR-29 family is the most consistently up-regulated during aging across multiple tissues [9], including the nervous system of multiple species [10–12], where it has been linked to age-related cognitive decline [13]. The role of miR-29 in brain maturation and aging is somewhat controversial. Even partial reduction of miR-29 reduces lifespan, induces neurodegeneration [14] and promotes brain aging hallmarks [4,8]. These results suggest that up-regulation of miR-29 family is linked to a compensatory response to limit age-related damage. On the other hand, however, overexpression of miR-29 has even been shown to induce premature aging in mice, suggesting that miR-29 is a driver of the aging process [15]. The miR-29 family, which includes miR-29a, miR-29b, and miR-29c, is encoded by two genomic loci: miR-29a/b-1 and miR-29b-2/c. Among these, miR-29a-3p (miR-29a) is particularly noteworthy, as it is the most upregulated during postnatal development and maturation of the mouse visual cortex [16] and its downregulation has been shown to slow cognitive decline and reduce beta-amyloid deposition [17]. This association suggests that miR-29a might play a pivotal role in the decline of cognitive function with aging. At the molecular level, miR-29a likely influences memory by modulating genes related to extracellular matrix and transcription regulation [16]. In particular, miR-29a directly targets DNA methyltransferases [18–20], which are responsible for adding methyl groups to DNA, thereby influencing gene activity. This modulation of DNA methylation pathways is particularly relevant in the context of aging, as changes in DNA methylation patterns have been linked to both aging and memory processes [21,22]. Rapid and dynamic changes in DNA methylation have been observed in response to neuronal activity [23,24], and studies have demonstrated that DNA methylation writers are necessary for learning and memory stability [25–27]. Moreover, within the brain-expressed miRNAs, miR-29a emerges as notably synaptically enriched [28], suggesting the involvement of miR-29a in the regulatory network underpinning

synaptic plasticity and the formation of memories [29]. However, the precise mechanisms through which miR-29a influences memory performance during development and in the adult brain remain elusive. In particular, whether the age-dependent increase in miR-29 expression is protective or disruptive for cognitive function is still to be ascertained. Our study shows that inhibiting miR-29a using LNA antagomirs resulted in increased Dnmt3a levels and improved memory retention, while enhancing miR-29a levels had the opposite effect. These findings suggest that miR-29a not only plays a role in age-related cognitive decline but also exerts a bidirectional control over memory possibly by altering the epigenetic landscape. Indeed, we observe increased CpG methylation in promoter and exon regions associated with CpG islands and modulation of the hippocampal transcriptome and proteome. Our findings provide compelling evidence that miR-29a orchestrates the molecular changes necessary for the maintenance of emotional memories, highlighting its potential role in age-related cognitive decline.

Results

Age-Dependent increase of miR-29a levels correlates with Dnmt3a reduction in the dorsal hippocampus

To investigate the temporal expression pattern of miR-29a in the dorsal hippocampus, we conducted a quantitative PCR (qPCR) analysis at different time points. Our results revealed a significant and remarkable 10-fold increase in miR-29a levels after postnatal day 10 (P10), reaching a plateau around P60 (Figure 1A). Interestingly, this specific temporal window aligns with critical periods characterized by heightened plasticity in various brain regions, accompanied by an increased sensitivity of chromatin configuration to environmental stimuli [30,31]. Simultaneously, we examined the age-related modulation of *Dnmt3a*, a well-validated target of miR-29 [19,32]. With increasing age, *Dnmt3a* expression showed a significant downregulation (Figure 1B), displaying a strong subject-by-subject negative correlation with miR-29a levels (Figure 1C). In a previous study, a comparable expression pattern was reported for the visual cortex, wherein the age-related elevation of miR-29a and decrease in *Dnmt3a* expression levels were associated with a significant decrease in ocular dominance plasticity and the expression of molecular critical period regulators [16]. Given that age-related decline in *Dnmt3a* levels has been proposed as a potential mechanism contributing to age-related cognitive impairments [33], we decided to explore the involvement of miR-29a in modulating fear memories. To evaluate whether and how the reduction in miR-29a

expression affects fear memory formation and extinction, we injected a locked nucleic acids (LNA) oligonucleotide, whose sequence is complementary to miR-29a (anti-miR29a), or scrambled oligonucleotide (scr) in the dorsal hippocampus of adult (P90) mice, and then we tested hippocampal memories through a hippocampus dependent trace fear conditioning protocol (TFC) (Figure 1D). As previously observed using LNA oligonucleotides against miR-29a in the visual cortex [16], anti-miR29a demonstrated a stable and specific binding affinity to their complementary miRNA, effectively blocking its activity, and exhibiting remarkable resistance to enzymatic degradation. These attributes render LNAs highly tolerable and validated, as underscored by their approval for clinical use in human subjects [34–36]. As expected, the qPCR revealed that anti-miR29a treatment caused a decrease in miR-29a (Figure 1E) and an increase in the *Dnmt3a* (Figure 1F). We also found a strong sample-by-sample negative correlation between *Dnmt3a* and miR-29a levels after LNA or scr injection (Figure S1A) confirming the tight regulation of *Dnmt3a* levels by miR-29a. To control for the spatial spreading of our treatment, we quantified *Dnmt3a* levels also in the ventral hippocampus. The results revealed no significant difference in *Dnmt3a* expression (Figure S1B), confirming the specificity of the injection effects within the dorsal hippocampus.

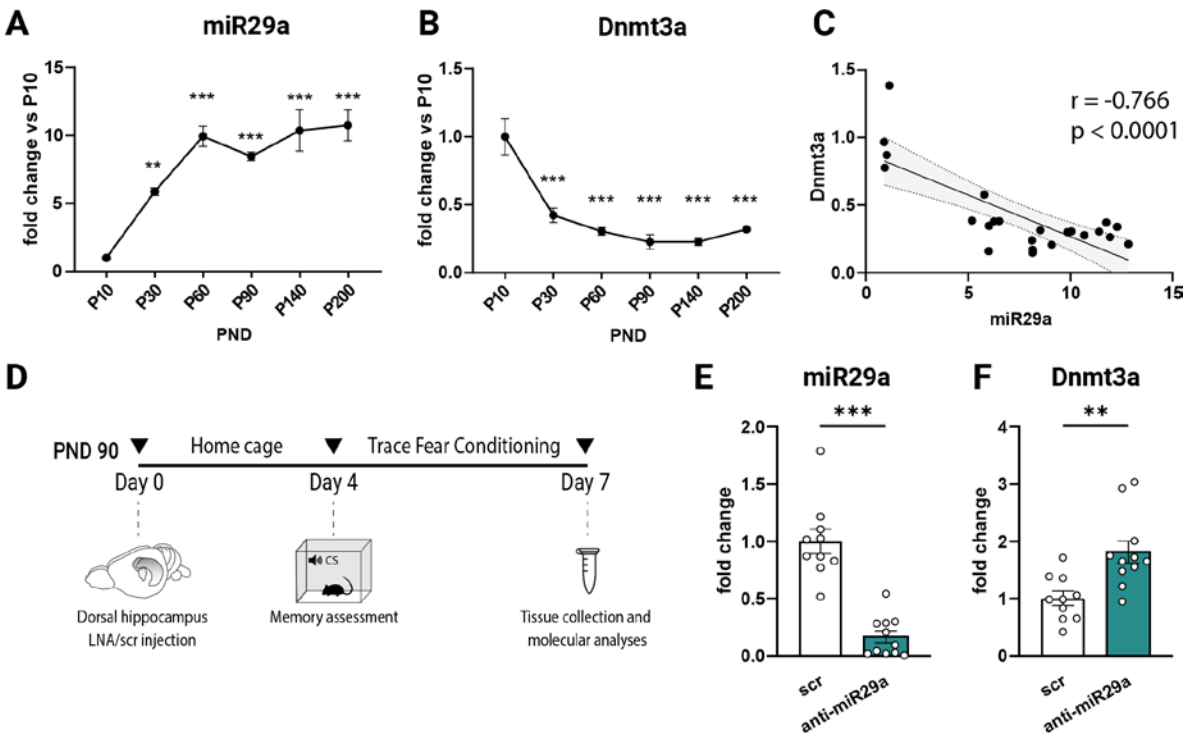

Figure 1: Correlation between age-dependent miR-29a increase and Dnmt3a. **(A)** Dorsal hippocampus miR-29a expression level (normalized to P10) at different ages (One-way ANOVA, P < 0.0001; Tukey's multiple comparison vs P10: **P < 0.01, ***P < 0.001 , n = 3/4 mice for each age).

(B) Dorsal hippocampus *Dnmt3a* expression level (normalized to P10) at different ages (One-way ANOVA, $P < 0.0001$; Sidak's multiple comparison vs P10: ***$P < 0.001$; n = 3/4 mice for each age). **(C)** Animal by animal correlation between normalized miR-29a and *Dnmt3a* levels in the dorsal hippocampus at different ages (Pearson's correlation). **(D)** Experimental design for LNA-anti-miR29a treatment in the dorsal hippocampus. **(E)** Effects of LNA-anti-miR29a treatment on miR-29a expression. Fold change values normalized to scr treated animals (scr: N = 10, anti-miR29a N = 11; Unpaired t-test: $p < 0.001$). **(F)** Effects of LNA-anti-miR29a treatment on *Dnmt3a* expression. Fold change values normalized to scr treated animals (scr: N = 10, anti-miR29a N = 11; Unpaired t-test: $p < 0.01$). PND = Postnatal Day.

MiR-29a downregulation promotes memory stability during fear extinction

Three days after anti-miR29a injection, we conditioned animals using a TFC protocol. During TFC the neutral conditioned stimulus (CS, Tone) and the aversive unconditioned stimulus (US, Shock) are separated in time by a trace interval (Trace). The absence of contiguity between the tone and the shock critically involves the hippocampus and this protocol can be used to evaluate hippocampal dependent learning and memory [37] (Figure 2A). We observed that the treatment did not affect learning acquisition, since both anti-miR29a and scr treated mice showed similar freezing during learning (Figure 2B and Figure S2A-C). When testing freezing responses 24 h after training, the two groups still did not differ in the percentage of time freezing (Figure 2D). However, on the first day of the extinction protocol (day 3, Early Extinction) we observed that anti-miR29a treated mice showed a higher fear retention, as compared to the control group (Figure 2E). This observation suggests that miR-29a developmental upregulation affects strength and persistence of memory, but it does not affect memory formation. We also assessed freezing behavior induced by exposure to the conditioned context (Figure 2A). Remarkably, mice subjected to anti-miR29a treatment exhibited a pronounced enhancement in their response to the contextual cues compared with the scr control group (Figure 2C). Despite this general amplification in fear response, anti-miR29a treated mice exhibited a typical extinction profile. Following the second extinction session (Late Extinction), both anti-miR29a and scr treated mice demonstrated significantly reduced freezing responses (Figure 2F). These findings suggest that elevated miR-29a levels impair memory stability, offering insights into miR-29a role in modulating the persistence of fear memories. This effect may be mediated through miR-29a's capacity to regulate DNA methylation patterns and influence gene expression.

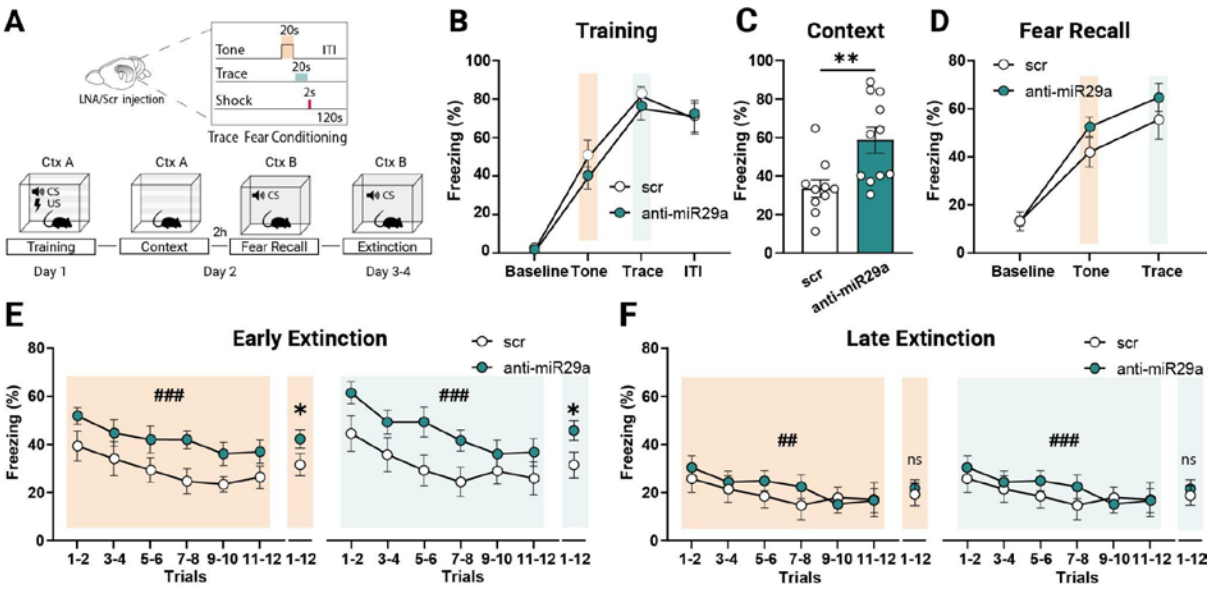

Figure 2: Reducing hippocampal miR-29a expression promotes memory stability. **(A)** Diagram showing the TFC paradigm and timeline. **(B)** Anti-miR29a and scr-treated animals showed no differences at baseline or in fear memory acquisition, as indicated by similar freezing responses during the final two-tone, trace trials and ITI of the TFC training session (Two-way ANOVA, test interval × treatment interaction $F(3, 76) = 0.39$, $p = 0.76$; main effect of test interval $F(3, 76) = 64.33$, $p < 0.0001$; main effect of treatment, $F(1, 76) = 0.93$, $p = 0.34$). **(C)** Downregulation of miR-29a in the dorsal hippocampus enhanced contextual memory recall (Unpaired t-test: $p < 0.01$, scr: N = 10, anti-miR29a N = 11). **(D)** No treatment differences were observed at baseline or during the final two-tone and trace trials of the TFC fear recall session (Two-way ANOVA, test interval × treatment interaction $F(2, 57) = 0.59$, $p = 0.56$; main effect of test interval $F(2, 57) = 41.74$, $p < 0.0001$; main effect of treatment, $F(1, 57) = 2.33$, $p = 0.13$). **(E)** Percentage of freezing during Early extinction. anti-miR29a mice showed a higher fear retention compared to the control group during both tone (Two-way RM ANOVA, main effect of treatment $F(1, 19) = 4.78$, $p < 0.05$; main effect of trials $F(2.98, 56.58) = 6.69$, $p < 0.0001$; trials × treatment interaction $F(5, 95) = 0.29$, $p = 0.92$) and trace intervals (Two-way RM ANOVA, main effect of treatment $F(1, 19) = 4.47$, $p < 0.05$; main effect of trials $F(3.26, 62.02) = 9.36$, $p < 0.0001$; trials × treatment interaction $F(5, 95) = 0.77$, $p = 0.57$). **(F)** During the Late extinction, anti-miR29a treated mice showed no significant differences in the percentage of freezing compared with controls (Tone: Two-way RM ANOVA, main effect of treatment $F(1, 18) = 0.19$, $p = 0.66$; main effect of trials $F(2.56, 46.16) = 4.81$, $p < 0.01$; trials × treatment interaction $F(5, 90) = 0.87$, $p = 0.50$; Trace: Two-way RM ANOVA, main effect of treatment $F(1, 18) = 0.24$, $p = 0.63$; main effect of trials $F(3.95, 71.15) = 6.26$, $p < 0.001$; trials × treatment interaction $F(5, 90) = 2.12$, $p = 0.07$). scr: N = 10, anti-miR29a N = 11; *indicates the main effect of treatment, #indicates the main effect of trials. CS= conditioned stumulus

MiR-29a inhibition alters DNA methylation patterns and influences memory-associated pathways at the transcript and protein level

We employed reduced representation bisulfite sequencing (RRBS) to investigate changes in DNA methylation patterns induced by anti-miR29a treatment in

comparison to scr treated hippocampal samples. RRBS allows for an exploration of methylation alterations in a CpG-enriched subset of the genome, primarily focusing on promoters [23,38]. We analyzed differential methylation of the sequenced CpGs and selected differentially-methylated CpGs (DMCs) with a difference greater than 10% in absolute value. Our analysis identified 2,279 DMCs, with a notable prevalence of hypermethylation (1,452 CpGs) over hypomethylation (827 CpGs, $p < 10\text{-}16$, Fisher's exact test, (Figure 3A and Dataset 1). These DMCs exhibited an even distribution across chromosomes and were enriched in promoter and exon regions, as well as within CpG islands (Figure 3B and Dataset 1). Interestingly, the observed increase in CpG methylation level after miR-29a inhibition is consistent with the increased expression of *Dnmt3a* (Figure 1F). To identify biological functions that may be influenced by increased *Dnmt3a* we performed a Gene Ontology (GO) term overrepresentation analysis on all DMCs identified as up-regulated. Analyzing the DMCs that fall within promoters, we found that most of the enriched biological processes relate to the regulation of gene expression via miRNA, splicing, and RNA metabolism and via CpG island methylation (Figure 3C and Dataset 2). This suggests miR-29a inhibition has a positive effect on gene expression by inhibiting repressive processes by increased methylation through *Dnmt3a*. Analyzing the DMCs that fall within the gene body, enrichment was found for extracellular matrix, protein tyrosine kinase activity, and notch activity, all mechanisms implicated in hippocampal-dependent learning and memory (Figure 3D and Dataset 3). In particular, tyrosine kinase receptor B (TrkB) is known to play a role in the acquisition and consolidation of fear memory [39]. With our methylation data, we confirmed the increase in methylation levels for TrkB following inhibition of miR-29a, providing further evidence for the involvement of this microRNA in the fear memory persistence pathway via modulation of *Dnmt3a* (Figure 3E). Notch pathway genes also appear to be characterized by increased methylation (Figure 3D): it has previously been shown that a decrease in Notch signaling, through miRNA regulation, is important for fear memory consolidation [40]. Overall, these findings confirm the central role of miR29 in orchestrating epigenetic mechanisms involved in memory persistence.

To investigate the possible downstream consequences of epigenetic changes we performed RNAseq and mass-spectrometry-based proteomics (Figure 4 and Dataset 4,5 respectively). The analysis of differentially expressed proteins retrieved 420 significant protein groups out of 4878 detected protein groups. To analyze the physical interaction of the the upregulated differentially-expressed proteins (DEPs, FDR <0.1, Log2(fold change) > 0.1), we applied STRING network analysis [41] and

found DEPss to be strongly connected (Figure 4 expected number of edges: 295; number of edges: 938; PPI enrichment p-value:< 1.0e-16). The protein network consisted almost entirely of two tightly clustered communities of functionally-interacting proteins: one made of synaptic proteins and the second of RNA binding proteins. A notable example is the upregulation of NMDA receptor subunits.

RNAseq detected 946 differentially expressed genes (DEGs). The analysis of the most overrepresented miRNA binding site in up-regulated DEGs revealed the expected enrichment for TGGTGCT (Webgestalt, FDR < 10-4), confirming effective antagonism of miR-29 family. STRING network analysis and found DEGs (FDR <0.1, DESeq2) to be strongly connected (Figure 4, expected number of edges: 345; number of edges: 660; PPI enrichment p-value:< 1.0e-16). Also the DEG network was strongly enriched for synaptic terms and RNA binding activity, indicating that the above-described regulation is transcriptionally-driven. STRING analysis of downregulated DEPs (FDR <0.1, Log2(fold change) <- 0.1) revealed a significantly connected network (expected number of edges: 142; number of edges: 260; PPI enrichment p-value:< 1.0e-16) with overrepresentation of terms related to immunity, myelin, mitochondria and ribosome. The analysis of downregulated DEGs (FDR <0.1, DESeq2) revealed a significantly connected network (expected number of edges:320 ; number of edges: 1482; PPI enrichment p-value:< 1.0e-16) with prominent overrepresentation of immunity-related terms and a interesting overrepresentation of the specific WiKI pathway WP3625 Tyrobp causal network in microglia. This network was identified by causal analysis of AD-driving mutations [42]. These data indicate that antagonism of miR-29 family dampens the inflammatory reaction induced by the injection via a transcriptional mechanism and reduces myelin, a major plasticity brake [43,44], via transcript-independent mechanisms.

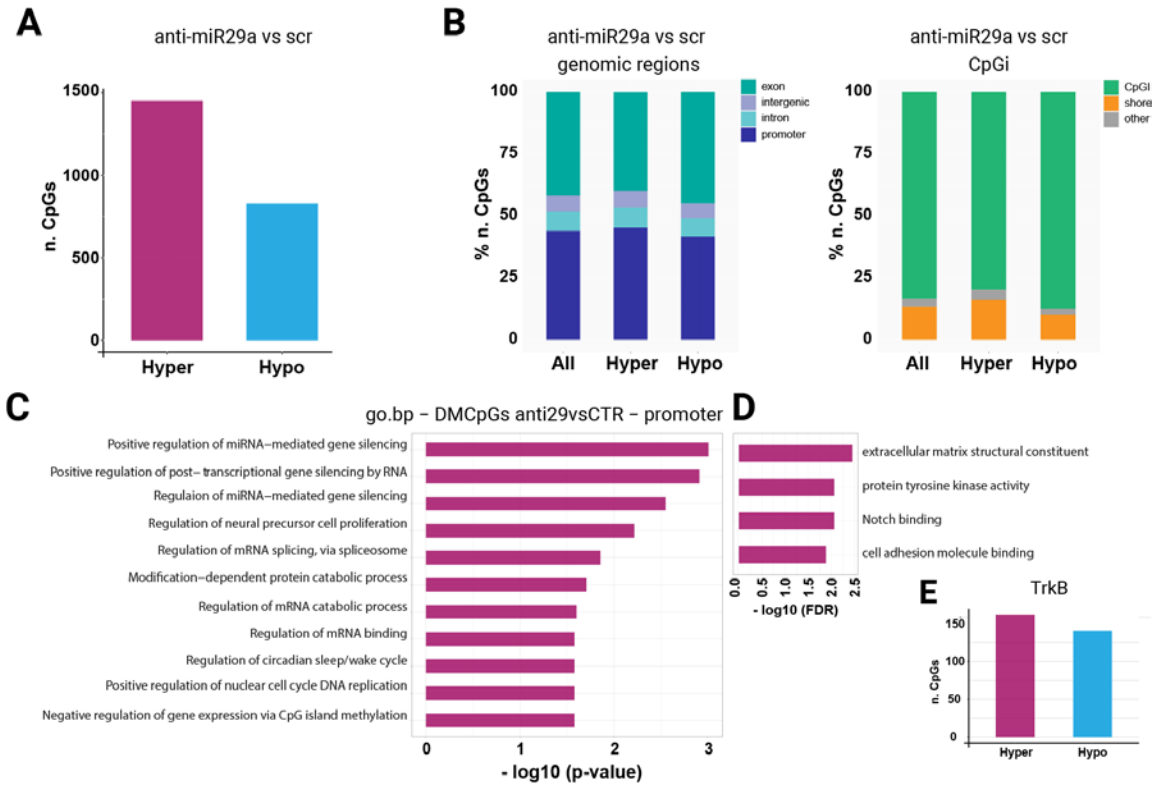

Figure 3: DNA methylation changes in the dorsal hippocampus after miR-29a downregulation. **(A)** The number of hyper- and hypo- methylated CpGs. We found 2,279 differentially-methylated CpGs (DMCs), with a prevalence of hypermethylation over hypomethylation (1,452 CpGs vs 827 CpGs, $p < 10\text{-}16$, Fisher's exact test) between anti29a and scr hippocampal treated samples. **(B)** DMCs distribution across chromosomes. DMCs exhibited an even distribution across chromosomes and were enriched in CpG island (CpGi). **(C-D)** GO term overrepresentation analysis on all the up-regulated DMCs **(C)** falling within promoters and **(D)** within the gene body. **(E)** Number of CpGs hyper- and hypo- methylated in TrkB. N=7 for each treatment.

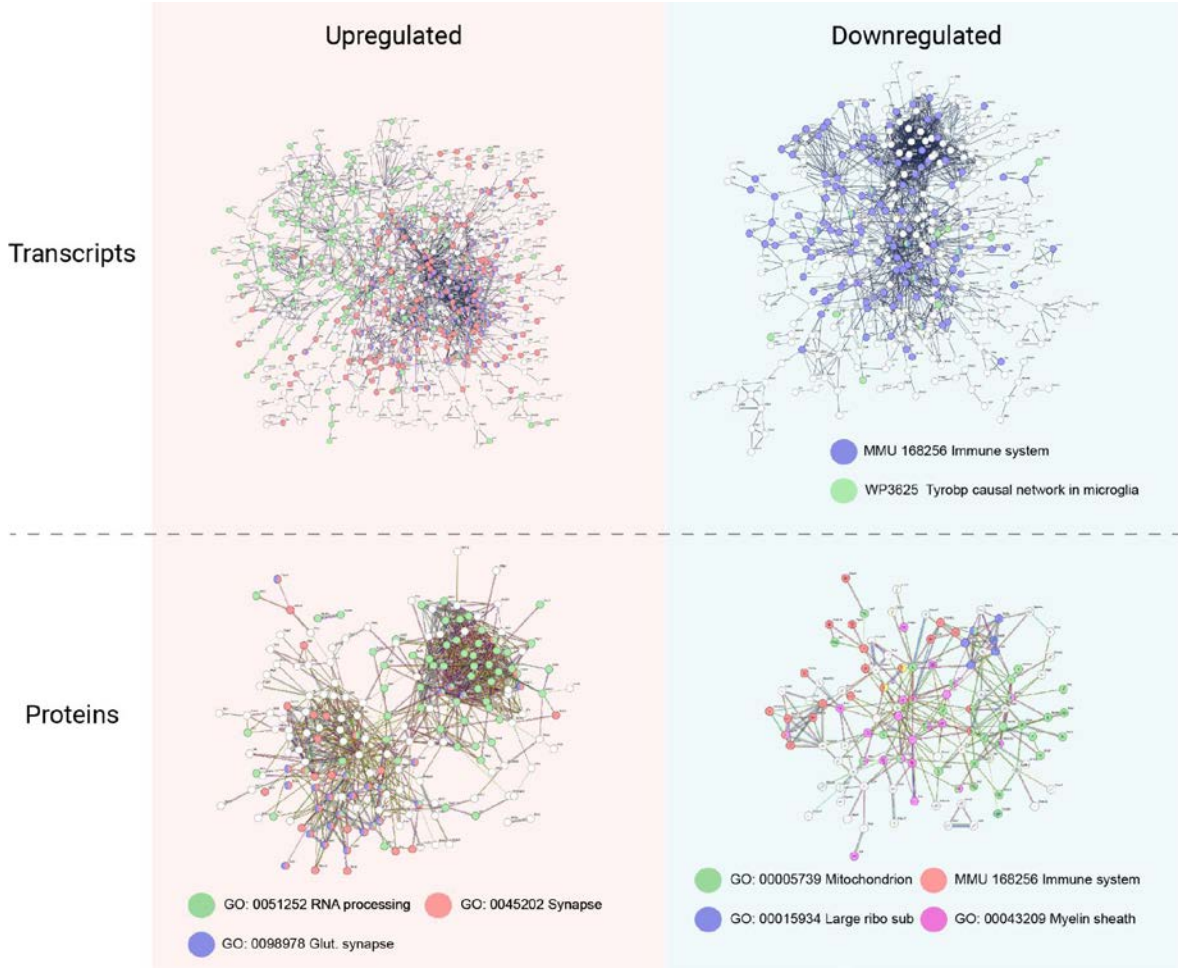

Figure 4: Transcriptomic and proteomic analysis of miR-29 antagonism. Each node represents a protein or transcript. The connections indicate functional interactions. Colors indicate selected GO terms. Analysis performed using STRING.

Elevated miR-29a levels in the hippocampus of adult mice result in impaired memory retention

To reveal whether miR-29a levels are quantitatively related to memory retention, we asked whether enhancing miR-29a levels in the dorsal hippocampus of adult mice could result in impaired retention. Before conditioning, we injected animals with a synthetic miR-29a mimic (mim29a) and then we tested defensive freezing responses using the same TFC protocol employed in the anti-miR29a experiments (Figure 5A). Mim29a treatment resulted in an upregulation of miR-29a expression and a concurrent downregulation of *Dnmt3a* levels in the dorsal (Figure 5B-C) but not in the ventral hippocampus (Figure S3) confirming the spatial selectivity and biological activity of the treatment. At the behavioral level, increasing miR-29a levels affected the trace stability but not the CS response. Indeed, during the extinction protocol

(Early Extinction) mim29a mice showed an impaired trace fear retention compared to the control group (Figure 5F). A trend toward a reduced response to the trace interval was also evident during both the training and recall phases (Figure 5D and Figure S4A-C). As observed also with anti-miR29a, mim29a treated mice displayed a normal extinction profile (Figure 5F-G).

The bidirectional impact of miR-29a on memory strength during the extinction was also evident for contextual memories. In particular, mice receiving miR-29a mimics displayed a strong deficit in the recall of contextual fear memories (Figure 5E) as compared to controls. The involvement of miR-29a in the maintenance of hippocampal fear memory stability was also confirmed by the presence of an inverse correlation between miR29a expression levels and the percentage of freezing behavior exhibited during early extinction and contextual fear recall (Figure 6A-E). Concurrently, a positive correlation was established between the expression levels of *Dnmt3a* and the percentage of freezing behavior manifested during the initial presentation of the trace interval in the early extinction Figure 6F. Overall, these findings support the hypothesis that heightened miR-29a levels and diminished expression of *Dnmt3a* contribute to the compromised stability of hippocampal fear memories [17,33,45].

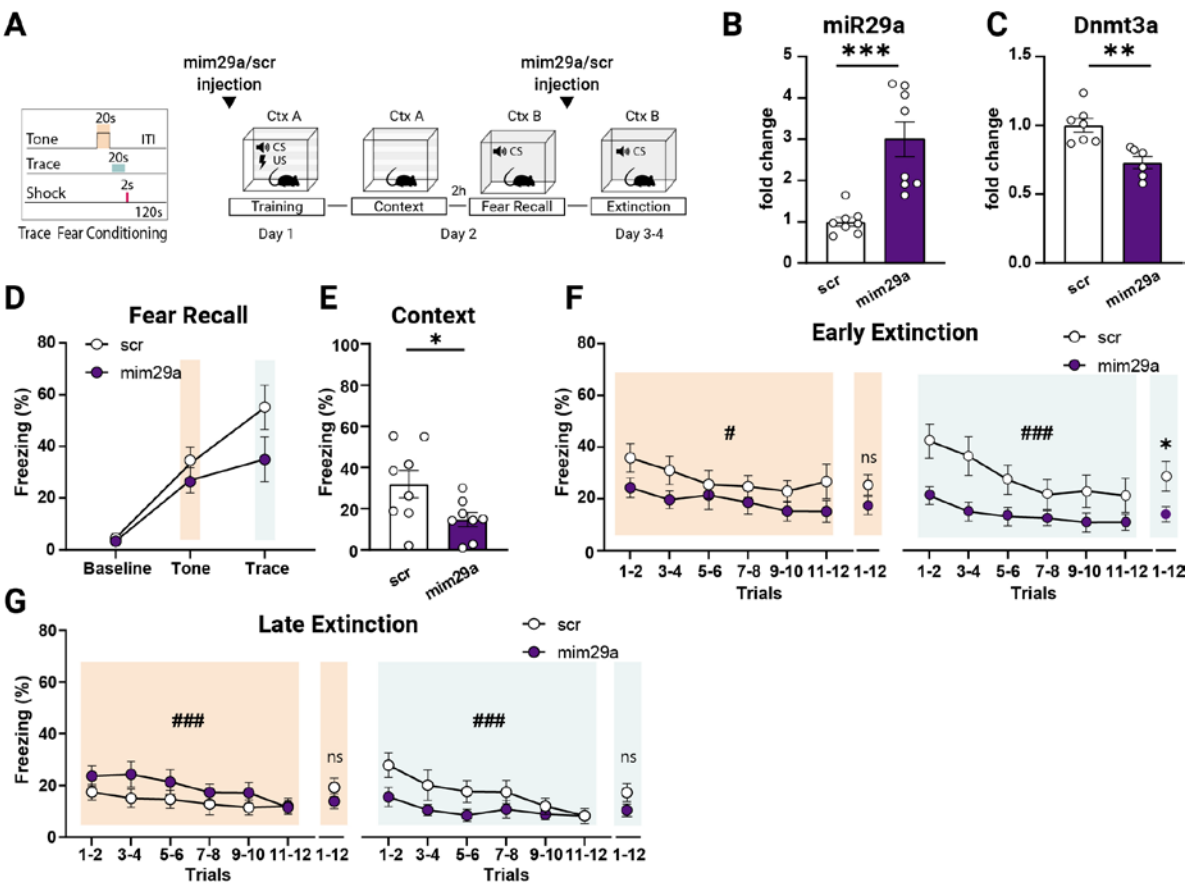

Figure 5: Hippocampal miR-29a upregulation impaired memory retention. **(A)** Diagram showing the TFC paradigm and timeline. To guarantee elevated miR-29a levels during all the sessions of the TFC test, mice were injected 24 hours before the start of the behavioral tests and again 24 hours before the start of the extinction protocol. **(B-C)** Effects of miR-29a mimic treatment on **(B)** miR-29a expression levels (fold change values normalized to scr treated animals; scr: N=8, mim29a N=8; Unpaired t-test: $p < 0.001$) and **(C)** *Dnmt3a* expression levels (fold change values normalized to scr treated animals; scr: N = 7, mim29a N = 6; Unpaired t-test: $p < 0.01$). **(D)** No treatment differences were observed at baseline or during the final two-tone and trace trials of the TFC fear recall session (Two-way ANOVA, test interval × treatment interaction $F(1, 42) = 3.52$, $p = 0.07$; main effect of test interval $F(2, 42) = 23.89$, $p < 0.0001$; main effect of treatment, $F(2, 42) = 1.30$, $p = 0.28$). **(E)** MiR-29a levels increase resulted in impaired contextual memory recall (Unpaired t-test: $p < 0.05$, scr: N = 8, miR-29a mimic N = 8). **(F)** Percentage of freezing during Early extinction. Mim29a treated mice showed lower fear retention compared to the control group during the trace (Two-way RM ANOVA, main effect of treatment $F(1, 19) = 4.475$, $p < 0.05$; main effect of trials $F(3.26, 62.02) = 9.365$, $p < 0.0001$; trials × treatment interaction $F(5, 95) = 0.77$, $p = 0.57$) but not during the tone interval (Two-way RM ANOVA, main effect of treatment $F(1, 14) = 2.30$, $p = 0.15$; main effect of trials $F(3.21, 44.97) = 3.80$, $p < 0.05$; trials × treatment interaction $F(5, 70) = 0.65$, $p = 0.66$). **(G)** During the Late extinction, mim29a treated mice showed no significant differences in the percentage of freezing compared with controls (Tone: Two-way RM ANOVA, main effect of treatment $F(1, 14) = 1.33$, $p = 0.27$; main effect of trials $F(3.63, 50.83) = 6.41$, $p < 0.001$; trials × treatment interaction $F(5, 70) = 1.46$, $p = 0.21$; Trace: Two-way RM ANOVA, main effect of treatment $F(1,14)) = 2.54$, $p = 0.13$; main effect of trials $F(3.35, 46.88) = 9.09$, $p < 0.0001$; trials × treatment interaction $F(5, 70) = 2.14$, $p = 0.07$). scr: N = 8, mim29a N = 8; *indicates the main effect of treatment, #indicates the main effect of trials.

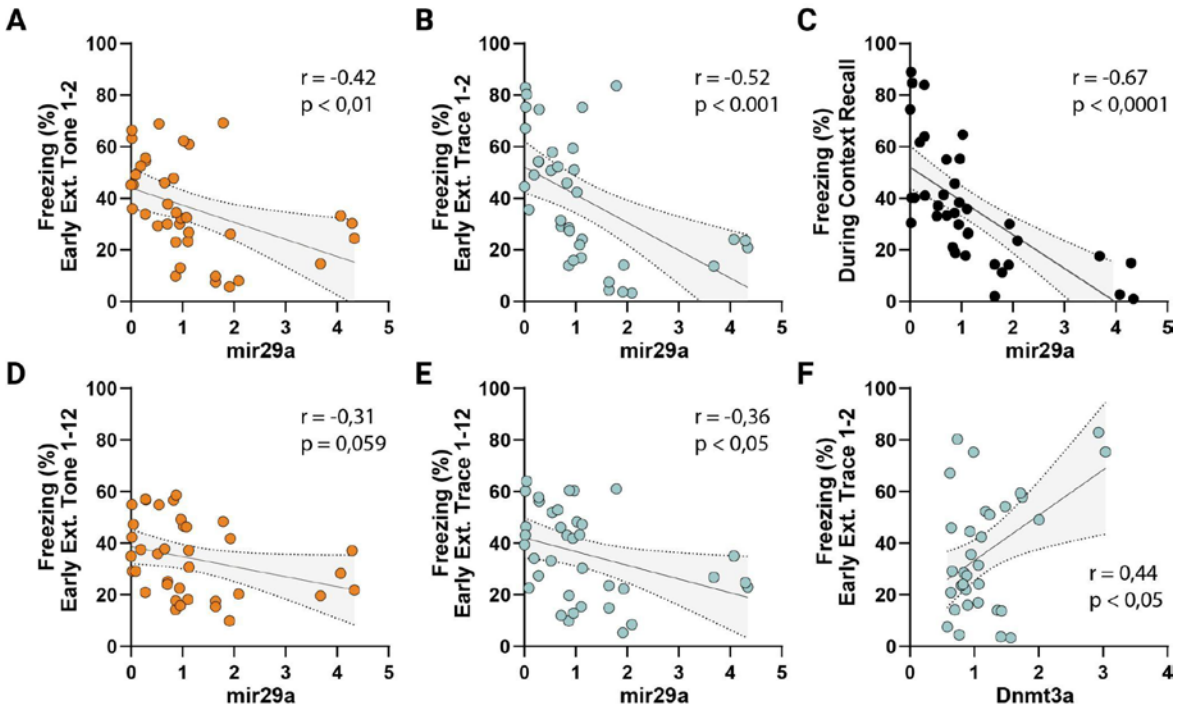

Figure 6: Behavioral correlation with miR-29a and *Dnmt3a* levels post LNA and mimic injection. **(A)** During early extinction miR-29a levels negatively correlate with freezing responses at the first two tone and **(B)** trace presentations (Pearson's correlation). **(C)** MiR-29a levels negatively correlate with freezing responses during contextual fear recall (Pearson's correlation). **(D)** During early extinction miR-29 levels do not correlate with freezing responses to the tone across all trials **(E)** but negatively correlate with freezing responses during the trace period across all trials (Pearson's correlation). **(F)** During early extinction *Dnmt3a* levels positively correlate with freezing responses at the first two trace presentations (Pearson's correlation).

Discussion

MiR-29 family regulation is characterized by a striking degree of conservation. Previous studies have demonstrated that miR-29a exhibits an age-associated upregulation across diverse species and tissues [11,12,46]. Furthermore, miR-29a plays a pivotal role in governing age-dependent processes such as neuronal maturation and iron accumulation within the brain [4,8]. In the visual cortex, miR-29a is the microRNA with the most significant upregulation during the visual critical period [10,16]. In addition, more than half of miR-29 predicted targets are downregulated with age, including key regulators of plasticity [16]. Our data confirmed this age-dependent upregulation of endogenous miR-29a expression in the dorsal hippocampus of wild-type mice, revealing a remarkable tenfold increase between P10 and P60. A previous study conducted in humans identified miRNAs linked to cognitive trajectories through a comprehensive global miRNA association study using postmortem brain samples [13]. Notably, among these miRNAs, higher levels of miR-29a emerged as the second miRNA most significant association with more rapid cognitive decline. These studies suggest that high levels of miR-29 are associated with reduced plasticity. To investigate the role of miR-29a function in influencing memory performances we bidirectionally modulate the levels of miR-29a in the dorsal hippocampus of adult mice. We found that the downregulation of miR-29a promotes hippocampal-dependent memory strength, while miR-29a upregulation impaired memory performances as observed during age-associated cognitive decline. The tight relationship between miR-29 levels and memory is emphasized by the negative correlation between miR-29a levels and the percentage of freezing observed during early extinction and contextual fear recall. Conversely, levels of *Dnmt3a* exhibited a positive correlation with the percentage of freezing exhibited in the initial stages of trace extinction. This finding lends support to the specific regulatory role of miR-29a in memory persistence. Recent work shows that miR-29a downregulation in the hippocampus of 5XFAD mice results in amelioration of

memory performances, reduction of beta-amyloid deposition, and lower microglia and astrocytes activation [17]. This effect of miR-29a downregulation in memory maintenance is coherent with its role as a master regulator of age-related molecular mechanisms.

miR- 29a sculpts the epigenetic landscape of adult hippocampus

Epigenetic mechanisms have been increasingly recognized as important regulators of cognitive functions through the modulation of transcriptional responses [47,48]. Since we found a strong negative correlation between miR-29a and *Dnmt3a* levels, we decided to explore the profile of methylation of anti-miR29a treated mice. DNA methylation is an essential epigenetic mechanism for various cellular processes and has emerged as a crucial regulator of memory consolidation [49,50]. Inhibition of miR-29a in the adult visual cortex reactivates ocular dominance plasticity in adult mice and upregulates genes associated with the extracellular matrix and epigenetic remodeling, however whether manipulations of miR-29 levels could result in global changes of DNA methylation was utterly unexplored. Contrary to what is observed for miR-29a levels, the degree of DNA methylation decreases with age in many tissues, including the nervous system [51,52]. In particular, aging has been associated with a reduction in the expression of the DNA methyltransferase *Dnmt3a2* in the hippocampus, and restoring *Dnmt3a2* levels has been shown to rescue cognitive functions affected by aging [33]. It has also been reported that hippocampal *Dnmt3a2* levels determine cognitive abilities in both young adult and aged mice [53]. Furthermore, DNA methylation induced selectively within neuronal ensembles has been proposed as a mechanism for stabilizing engrams during consolidation, supporting successful memory retrieval [54]. After miR-29a inhibition, we found an increase in CpG methylation level, consistent with the measured increased expression of *Dnmt3a*. Moreover, the GO analysis conducted on all the up-regulated DMCs, revealed for the DMCs that fall in promoters, an enrichment in biological processes related to regulation of gene expression. This suggests that miR-29a inhibition has a positive effect on gene expression by inhibiting repressive processes via increased methylation. For the DMCs that fall within the gene body, enrichment was found for mechanisms implicated in hippocampal-dependent learning and memory such as the Notch and TrkB. The Notch pathway stands as one of the most highly conserved signaling cascades governing cellular communication, cell fate determination, and morphogenetic processes, exerting its influence from early development onwards [55,56]. Multiple investigations have demonstrated the fundamental role of Notch signaling in neurophysiological phenomena, including learning and memory, across various species, including mammals [57]. Moreover,

research has unveiled compromised Notch signaling within the brains of Alzheimer's disease patients, implying a potential causal link between alterations in Notch function and memory impairment [58]. Recent experimental evidence substantiates BDNF's involvement in memory functions [59], where both memory acquisition and consolidation correlate with elevated BDNF mRNA expression [60] and the activation of its receptor, TrkB [61]. Genetic or pharmacological depletion of BDNF or TrkB has been shown to impair learning and memory [62,63]. Although our data showed hypermethylation of these pathways, it is noteworthy that, in contrast to the typical association between promoter methylation and gene repression, gene body methylation is positively correlated with gene expression [64,65]. Overall, our results shed light on the intricate interplay between miR-29a and plasticity-related epigenetic mechanisms, specifically within the context of memory persistence. Further exploration of these molecular pathways holds great promise for advancing our understanding of memory consolidation and the development of potential therapeutic strategies for memory-related disorders. Our proteomic and transcriptomic studies further validate a prominent role of miR-29 in regulating gene expression as RNA binding-proteins were upregulated after miR-29 antagonism in a process that was driven by transcriptional control. Similarly, synaptic proteins and their transcripts were upregulated, identifying a molecular correlate of enhanced plasticity that is further highlighted by upregulation of NMDA receptors. Notably, up-regulation of glutamatergic synaptic proteins was previously detected also in the visual cortex after miR-29 antagonism[16]. Analysis of down-regulated transcripts and proteins reveal a prominent effect of inflammation and activation of the microglia. These results suggest that antagonism of miR-29 reduces the reactive response induced by the injection and it is in line with the well-known effect of miR-29 on the immune system [6,66,67]. Some other protein changes appear to be transcription-independent, such as the down-regulation of myelin proteins. Myelin proteins are extremely long-lived [68] and therefore rapid transcriptional control of their expression is not possible. Myelin represents a well-described plasticity brake [43,44] and reduced myelin may enable learning associated plasticity after miR-29 antagonism. In light of the promising findings in our current study, it merits consideration to contemplate future experiments that involve a more extensive exploration of the relationship between memory persistence and miR-29a levels during development. Specifically, performing behavioral analyses at various ages characterized by distinct miR-29a levels could offer valuable insights into the dynamics of this correlation across different developmental stages.

Resource availability

Lead contact

Further information and requests for resources and reagents should be directed to the lead contact, Tommaso Pizzorusso (tommaso.pizzorusso@sns.it).

Materials availability

This study did not generate new unique reagents.

Data and code availability

- All data reported in the main text or supplemental information are available from the lead contact upon request.
- All original code is also available from the lead contact upon request.
- Any additional information required to reanalyze the data reported in this paper is available from the lead contact upon request.

Acknowledgments

We gratefully acknowledge NVIDIA Corporation's support with the Jetson AGX Xavier Developer Kit donation for this research. Funded by the European Union - Next Generation EU Missione 4 Componente 2 Inv. 1.5 CUP I53C22000780001 and PRIN2022 20228RMXBE to T.P.

Author contributions

Conceptualization: AV, AC, TP

Methodology: AV, EP, CG, RM, AC, TP

Formal analysis: AV, CG, AC,

Investigation: AV,CG,EP

Resources: AC, TP, RM

Data curation: AV, AC

Writing original draft: AV, AC, TP

Visualization: AV, AC

Supervision: TP, AC

Project administration: TP, AC

Funding acquisition: TP, AC

Declaration of interests

The authors declare no competing interests.

Experimental Procedures

Animals

All experiments utilized both male and female mice of the C57BL/6J strain. Animals were maintained at 22°C under a 12-h light–dark cycle (average illumination levels of 1.2 cd/m2) and housed in standard cages according to current regulations about animal welfare. Food (4RF25 GLP Certificate, Mucedola) and water were available ad libitum. All the experiments were carried out according to the directives of the European Community Council (2011/63/EU) and approved by the Italian Ministry of Health (621/2020-PR). All tissue explants were performed at the same time of the day (10–12 am).

Stereotaxic surgery

Mice were anesthetized and fixed on stereotaxic support through the use of metal bars in the ears. The skin was removed, and perforations were produced in the skull using a surgical drill. We injected an LNA oligonucleotide, whose sequence is complementary to miR-29a (miR-29a-3p miRCURY LNA, QIAGEN, Cat. No: 339121, 50µM) and a synthetic miR-29a mimic (mirVanaTM miRNA miR-29a-3p Mimic, ThermoFisher, Cat. No: 4464066, 100µM), or scrambled sequences as control. Injection in the dorsal hippocampus was done using the following stereotaxic coordinates: –2 mm anteroposterior, ±1.5 mm mediolateral, –1.5, –1.7 mm dorsoventral from bregma. A total of 2 µl of solution per hemisphere was injected, 1µl for each coordinate. The injection needle was left in place for an additional 60 s to allow the fluid to diffuse. The skin was subsequently sutured, and a physiological solution was injected subcutaneously to prevent dehydration. Paracetamol was administered in water ad libitum for two days. Due to the inherent stability of LNA oligonucleotides, a singular injection was administered to mice before the beginning of the behavioral test. In contrast, the miR-29a mimic exhibited faster degradation within a specific three-day timeframe (data not shown). To maintain the levels of miR-29a consistently elevated during all the sessions of the behavioral test, mice received injections every two days.

Trace fear conditioning and extinction protocol

Mice were subjected to a trace fear conditioning and extinction procedure using a custom-made PVC fear conditioning setup (50 cm X 15 cm X 21 cm). During the test days, the mice were transported in their home cages to a room adjacent to the testing room and left for 2 h before behavioral testing. We used two different contexts: In context A, the walls had white plastic circles and the floor was

completely black; in context B, the walls had white vertical plastic strips and a white floor. Both chambers were covered with transparent plexiglass lids with a loudspeaker in its center point. The shock grid on the floor was made of stainless steel. Only the grid of context A was electrified by a shock generator (World Precision Instruments, Sarasota, FL) and guided by an Arduino Uno for CS and US parameter control and footshock delivery. Mice behavior was recorded by a camera controlled by the EthoVision XT 8 software (Noldus Information Technology, The Netherlands). The apparatus was cleaned before and after each animal with 70% ethanol or 1% acetic acid for context A and context B respectively, since the mice may associate the smell with the context. After each session, mice were housed separately until the end of the test to avoid possible observational fear learning. During the Training phase of the test (Day 1), mice were allowed to explore the conditioning chamber (Context A) for 2 min (baseline) before receiving five conditioning trials. Each trial consisted of a 20 s pure tone (80 dB, 2900 Hz) and a 2 s shock (0.6 mA) separated by a 20 s stimulus-free trace interval. The intertrial interval (ITI) was 120 s. Mice were removed from the chamber 120 s after the last trial. Twenty-four hours later (Day 2), mice were placed back in the conditioning chamber (Context A) for a 5 min context test. The same day (Day2) after 2 h from the context test, mice were placed in a different contest (Context B) for a Recall test consisting of a 2 min baseline period followed by four 20 s tone presentations separated by a 20 s stimulus-free trace interval with 120 s ITI. On day 3 (Early Extinction) and day 4 (Late Extinction), conditioned mice were subjected to the extinction training in context B during which they received twelve 20 s tone presentations separated by 20 s stimulus-free trace interval presentations with 120 s ITI each day.

Analysis of Freezing Behavior

Recorded videos were manually scored for freezing behavior by two separate experimenters blind to treatment conditions. Mice were considered to be freezing if no movement was detected for 2 s (defined as the complete absence of movement except for respiratory movements). Evoked freezing behavior was analyzed by calculating the percentage of time an animal spent freezing during a given phase of the test. During fear extinction, averages were calculated by pooling freezing across 2 CS presentations if not indicated otherwise.

RNA extraction and quantification (qPCR)

Tissue samples were homogenized in the cell disruption buffer (Ambion). RNA was extracted by the addiction of Phenol/guanidine-based QIAzol Lysis Reagent

(Qiagen, cat. no. 79306). Chloroform was added, and the samples were shaken for 15 s. The samples were left at 20–24°C for 3 min and then centrifuged (12,000 g, 20 min, 4°C). The upper phase aqueous solution, containing RNA, was collected in a fresh tube, and the RNA was precipitated by the addition of isopropanol. Samples were mixed by vortexing, left at 20–24°C for 15 min, and then centrifuged (12,000 g, 20 min, 4°C). The supernatant was discarded, and the RNA pellet was washed in 75% ethanol by centrifugation (7500 g, 10 min, 4°C). The supernatant was discarded, and the pellet was left to dry for at least 15 min; then, it was resuspended in RNAse-free water. Total RNA concentrations were determined by NanoDrop Spectrophotometer (Thermo Scientific 2000 C). RNA quality was analyzed through a gel running (1% agarose). Total RNA was reverse transcribed using the QuantiTeck Reverse Transcription Kit (Qiagen, cat. no. 205311), and miRNAs were reverse transcribed using the TaqMan MicroRNA reverse transcription kit (Thermo Fisher, cat. no. 4366596). Gene expression was analyzed by real-time PCR (Step one, Applied Biosystems). TaqMan inventoried assays were used for miR-29a-3p (assay ID: 002112), sno234 (assay ID:001234), and Dnmt3a (Mm00432881 m1). TaqMan assay was used for glyceraldehyde 3-phosphate dehydrogenase (Gapdh), GAPDH probe ATCCCAGAGCTGAACGG, GADPH forward CAAGGCTGTGGGCAAGGT, and GADPH reverse GGCCATGCCAGTGAGCTT. Quantitative values for cDNA amplification were calculated from the threshold cycle number (Ct) obtained during the exponential growth of the PCR products. The threshold was set automatically by the Step One software. Data were analyzed by the ΔΔCt methods using GAPDH or SNO234 to normalize the cDNA levels of the transcripts under investigation.

DNA extraction and validation

For the methylation analysis, we administered LNA-anti-miR29a to one hemisphere of seven mice, while the other hemisphere received an injection of the scrambled sequence, serving as an internal control. To mitigate potential lateralization effects, we randomized the side of LNA injection. Seven days after the injection, tissues

were collected and samples were stored in an ultralow freezer (-80°C) until DNA extraction. DNA was isolated from snap-frozen hippocampi using the QIAamp DNA Micro Kit (Qiagen) following the manufacturer's protocol. DNA concentration was measured with NanoDrop 2000 (Thermo Scientific), using 1 µl of input DNA. Then, dsDNA concentration was quantified using Quant-iT Picogreen dsDNA Assay (Thermo Scientific), and the distribution of DNA fragments was assessed by TapeStation 4200 (Agilent).

RRBS method

RRBS libraries were produced by Ovation RRBS Methyl-Seq with the TrueMethyl oxBS kit (Tecan, Redwood City, CA, USA) according to the manufacturer's instructions. Briefly, 100 ng of genomic DNA was digested for 1h at 37°C with the methylation-insensitive restriction enzyme MpsI. Then, fragments were ligated to methylated adapters and treated with bisulfite to convert unmethylated cytosine into uracil. PCR amplification was then performed to obtain the final DNA library. The resulting libraries were sequenced on the Illumina NovaSeq6000 with 100 bp single-end sequencing with an average of 60 million reads per sample.

RRBS data analysis

The sequencing reads were trimmed to remove the adapter and low-quality bases with Trim Galore! (www.bioinformatics.babraham.ac.uk). Then trimmed reads were aligned to the mouse reference genome mm39 with BSMAPz (github.com/zyndagj). Using the Python script methratio.py in BSMAPz, methylation ratios were extracted from the mapping output. Methylation analysis was performed using the R package methylKit (version 1.20.0) (Akalin et al., 2012). Only CpGs covered by at least 10 reads and present in every sample were retained for downstream analysis. The methylation ratio of each site was calculated by dividing the number of reads called "C" by the total number of reads called either "C" or "T" at the specific site. The methylation score for each CpG site is represented as a β-value which ranges between 0 (unmethylated) and 1 (fully methylated). Differentially methylated CpGs (DMCs) were detected using a logistic regression model based on a Chi-square test. A false discovery rate (FDR) q value threshold of < 0.05 and methylation difference of ±10% between treated and control groups was used to identify significant DMCs. The promoter was defined as the region ±1kb from the transcription start site. Pathway analysis was performed using the web tools WebGestalt (www.webgestalt.org) and EnrichR (maayanlab.cloud).

Sample preparation for proteomics analysis

Before lysis, a lysis buffer (fc 4% SDS, 100 mM HEPES, pH 8.5, 50 mM DTT) was added to each sample. Samples were then boiled at 95°C for 7 min and sonicated using a tweeter. Reduction was followed by alkylation with 200 mM iodoacetamide (IAA, final concentration 15 mM) for 30 min at room temperature in the dark. Samples were acidified with phosphoric acid (final concentration 2.5%), and seven times the sample volume of S-trap binding buffer was added (100 mM TEAB, 90% methanol). Samples were bound on a 96-well S-trap micro plate (Protifi) and washed three times with a binding buffer. Trypsin in 50 mM TEAB pH 8.5 was added to the samples (1 µg per sample) and incubated for 1 h at 47°C. The samples were eluted in three steps with 50 mM TEAB pH 8.5, elution buffer 1 (0.2% formic acid in water) and elution buffer 2 (50% acetonitrile and 0.2% formic acid). The eluates were dried using a speed vacuum centrifuge (Eppendorf Concentrator Plus, Eppendorf AG, Germany) and stored at -20° C. Before analysis, samples were reconstituted in MS Buffer (5% acetonitrile, 95% Milli-Q water, with 0.1% formic acid) and spiked with iRT peptides (Biognosys, Switzerland).

LC-MS Data independent analysis (DIA)

Peptides were separated in trap/elute mode using the nanoAcquity MClass Ultra-High Performance Liquid Chromatography system (Waters, Waters Corporation, Milford, MA,USA) equipped with a trapping (Waters nanoEase M/Z Symmetry C18, 5µm, 180 µm x 20 mm) and an analytical column (Waters nanoEase M/Z Peptide C18, 1.7µm, 75µm x 250mm). Solvent A was water and 0.1% formic acid, and solvent B was acetonitrile and 0.1% formic acid. 1 µl of the sample (~1 µg on column) was loaded with a constant flow of solvent A at 5 µl/min onto the trapping column. Trapping time was 6 min. Peptides were eluted via the analytical column with a constant flow of 0.3 µl/min. During the elution, the percentage of solvent B increased in a nonlinear fashion from 0–40% in 120 min. Total run time was 145 min. including equilibration and conditioning. The LC was coupled to an Orbitrap Exploris 480 (Thermo Fisher Scientific, Bremen, Germany) using the Proxeon

nanospray source. The peptides were introduced into the mass spectrometer via a Pico-Tip Emitter 360-µm outer diameter × 20-µm inner diameter, 10-µm tip (New Objective) heated at 300 °C, and a spray voltage of 2.2 kV was applied. The capillary temperature was set at 300°C. The radio frequency ion funnel was set to 30%. For DIA data acquisition, full scan mass spectrometry (MS) spectra with mass range 350–1650 m/z were acquired in profile mode in the Orbitrap with resolution of 120,000 FWHM. The default charge state was set to 3+. The filling time was set at a maximum of 60 ms with a limitation of 3 × 10 6 ions. DIA scans were acquired with 40 mass window segments of differing widths across the MS1 mass range. Higher collisional dissociation fragmentation (stepped normalized collision energy; 25, 27.5, and 30%) was applied and MS/MS spectra were acquired with a resolution of 30,000 FWHM with a fixed first mass of 200 m/z after accumulation of 3 × 10 6 ions or after filling time of 35 ms (whichever occurred first). Data were acquired in profile mode. For data acquisition and processing of the raw data Xcalibur 4.3 (Thermo) and Tune version 2.0 were used.

Proteomic data processing

DIA raw data were analyzed using the directDIA pipeline in Spectronaut v.18 (Biognosys, Switzerland) with BGS settings besides the following parameters: Protein LFQ method = QUANT 2.0, Proteotypicity Filter = Only protein group specific, Major Group Quantity = Median peptide quantity, Minor Group Quantity = Median precursor quantity, Data Filtering = Qvalue, Normalizing strategy = Local Normalization. The data were searched against a UniProt (Mus musculus, v. 160106, 16.748 entries) and a contaminants (247 entries) database. The identifications were filtered to satisfy FDR of 1 % on peptide and protein level. Relative protein quantification was performed in Spectronaut using a pairwise t-test performed at the precursor level followed by multiple testing correction according to Benjamini-Hochberg.

RNA-Seq library preparation

Sequencing of RNA samples was done using Illumina's next-generation sequencing methodology . In detail, quality check and quantification of total RNA was done using the Agilent Bioanalyzer 2100 in combination with the RNA 6000 pico kit (Agilent Technologies, 5067-1513). Total RNA library preparation was done by introducing 500 ng total RNA into Illumina's NEBNext Ultra II directional mRNA (UMI) kit (NEB, E7760S), following the manufacturer's instructions. The quality and quantity of all libraries were checked using Agilent's Bioanalyzer 2100 and DNA 7500 kit (Agilent Technologies, 5067-1506).RNAseq analysis. All libraries were sequenced on a NovaSeq6000 SP 100 cycles v1.5. Corresponding UMI file was used to add UMI sequences to the reads names of each sample R1 file using UMI-tools extract v1.1.1 [69] to enable duplicate removal in the later steps. Trimmomatic v0.36 [70] was applied to the reads to remove adapters and low quality sequences using custom adapter fasta file and the following options adapters_3tools.fa:2:30:10:6 SLIDINGWINDOW:3:25 MINLEN:25. Trimmed reads were then mapped onto the *Mus musculus* GRCm39 genome primary assembly from Ensembl release 111 [71] using STAR v2.7.10a [72] and -outSAMtype BAM SortedByCoordinate -outSAMmultNmax 1 --outSJfilterReads Unique --outSAMstrandField intronMotif --alignIntronMax 100000 --outFilterMismatchNoverLmax 0.04 options to generate sorted bam files. The resulting bam file was indexed using samtools v1.19.2-23-g1a63877 [73] and duplicates were removed from it using UMI-tools dedup v1.1.1 [74]. In order to get gene-level counts for each sample featureCounts v2.0.3 [75] was used with mouse GRCm39 GTF annotation from Ensembl release 111 [76] and -s 2 flag. Counts from individual samples were then combined into a single counts matrix for use in downstream analysis tools.

Differential expression Analysis

Differential expression analysis was performed using DESeq2 [77]. Exploratory data analysis was performed with PCA to identify possible outliers. Counts were normalized by variance stabilizing transformation (vst) and adaptive fold-change shrinkage (apeglm). Differential expression analysis was performed with default parameters. Since samples are paired, the following design was implemented: design = ~ Subject + Cond where Cond has two categorical values = "Scramble" and "anti-miR-29".

Statistical analysis

All the statistical analyses were performed using GraphPad Prism 8. Parametric t-test, Pearson's correlation, analysis of variance (ANOVA), and repeated measure-ANOVA (RM-ANOVA) were used. ANOVA was followed by appropriate post hoc tests. Significance was set at $P<0.05$ for all tests. Error bars represent s.e.m. in all figures.

References

1. Bartel, D.P. (2018). Metazoan MicroRNAs. Cell *173*, 20–51.

2. Rajman, M., and Schratt, G. (2017). MicroRNAs in neural development: from master regulators to fine-tuners. Development *144*, 2310–2322.

3. Lippi, G., Fernandes, C.C., Ewell, L.A., John, D., Romoli, B., Curia, G., Taylor, S.R., Frady, E.P., Jensen, A.B., Liu, J.C., et al. (2016). MicroRNA-101 Regulates Multiple Developmental Programs to Constrain Excitation in Adult Neural Networks. Neuron *92*, 1337–1351.

4. Kole, A.J., Swahari, V., Hammond, S.M., and Deshmukh, M. (2011). miR-29b is activated during neuronal maturation and targets BH3-only genes to restrict apoptosis. Genes Dev. *25*, 125–130.

5. Dalgaard, L.T., Sørensen, A.E., Hardikar, A.A., and Joglekar, M.V. (2022). The microRNA-29 family: role in metabolism and metabolic disease. Am. J. Physiol. Cell Physiol. *323*, C367–C377.

6. Ma, F., Xu, S., Liu, X., Zhang, Q., Xu, X., Liu, M., Hua, M., Li, N., Yao, H., and Cao, X. (2011). The microRNA miR-29 controls innate and adaptive immune responses to intracellular bacterial infection by targeting interferon-γ. Nat. Immunol. *12*, 861–869.

7. Yee Mon, K.J., Zhu, H., Daly, C.W.P., Vu, L.T., Smith, N.L., Patel, R., Topham, D.J., Scheible, K., Jambo, K., Le, M.T.N., et al. (2021). MicroRNA-29 specifies age-related differences in the CD8+ T cell immune response. Cell Rep. *37*, 109969.

8. Ripa, R., Dolfi, L., Terrigno, M., Pandolfini, L., Savino, A., Arcucci, V., Groth, M., Terzibasi Tozzini, E., Baumgart, M., and Cellerino, A. (2017). MicroRNA miR-29 controls a compensatory response to limit neuronal iron accumulation during adult life and aging. BMC Biol. *15*, 9.

9. Wagner, V., Kern, F., Hahn, O., Schaum, N., Ludwig, N., Fehlmann, T., Engel, A., Henn, D., Rishik, S., Isakova, A., et al. (2024). Characterizing expression changes in noncoding RNAs during aging and heterochronic parabiosis across mouse tissues. Nat. Biotechnol. *42*, 109–118.

10. Mazziotti, R., Baroncelli, L., Ceglia, N., Chelini, G., Sala, G.D., Magnan, C., Napoli, D., Putignano, E., Silingardi, D., Tola, J., et al. (2017). Mir-132/212 is required for maturation of binocular matching of orientation preference and depth perception. Nat. Commun. *8*, 15488.

11. Somel, M., Guo, S., Fu, N., Yan, Z., Hu, H.Y., Xu, Y., Yuan, Y., Ning, Z., Hu, Y., Menzel, C., et al. (2010). MicroRNA, mRNA, and protein expression link development and aging in human and macaque brain. Genome Res. *20*, 1207–1218.

12. Baumgart, M., Groth, M., Priebe, S., Appelt, J., Guthke, R., Platzer, M., and Cellerino, A. (2012). Age-dependent regulation of tumor-related microRNAs in the brain of the annual fish Nothobranchius furzeri. Mech. Ageing Dev. *133*, 226–233.

13. Wingo, A.P., Wang, M., Liu, J., Breen, M.S., Yang, H.-S., Tang, B., Schneider, J.A., Seyfried, N.T., Lah, J.J., Levey, A.I., et al. (2022). Brain microRNAs are associated with variation in cognitive trajectory in advanced age. Transl. Psychiatry *12*, 47.

14. Papadopoulou, A.S., Serneels, L., Achsel, T., Mandemakers, W., Callaerts-Vegh, Z.,

Dooley, J., Lau, P., Ayoubi, T., Radaelli, E., Spinazzi, M., et al. (2015). Deficiency of the miR-29a/b-1 cluster leads to ataxic features and cerebellar alterations in mice. Neurobiol. Dis. *73*, 275–288.

15. Swahari, V., Nakamura, A., Hollville, E., Hung, Y.-H., Kanke, M., Kurtz, C.L., Caravia, X.M., Roiz-Valle, D., He, S., Krishnamurthy, J., et al. (2024). miR-29 is an important driver of aging-related phenotypes. Commun Biol *7*, 1055.

16. Napoli, D., Lupori, L., Mazziotti, R., Sagona, G., Bagnoli, S., Samad, M., Sacramento, E.K., Kirkpartick, J., Putignano, E., Chen, S., et al. (2020). MiR-29 coordinates age-dependent plasticity brakes in the adult visual cortex. EMBO Rep. *21*, e50431.

17. Mei, Z., Liu, J., Schroeder, J.P., Weinshenker, D., Duong, D.M., Seyfried, N.T., Li, Y., Jin, P., Wingo, A.P., and Wingo, T.S. (2024). Lowering Hippocampal miR-29a Expression Slows Cognitive Decline and Reduces Beta-Amyloid Deposition in 5×FAD Mice. Mol. Neurobiol. *61*, 3343–3356.

18. Swahari, V., Nakamura, A., Hollville, E., Stroud, H., Simon, J.M., Ptacek, T.S., Beck, M.V., Flowers, C., Guo, J., Plestant, C., et al. (2021). MicroRNA-29 is an essential regulator of brain maturation through regulation of CH methylation. Cell Rep. *35*, 108946.

19. Fabbri, M., Garzon, R., Cimmino, A., Liu, Z., Zanesi, N., Callegari, E., Liu, S., Alder, H., Costinean, S., Fernandez-Cymering, C., et al. (2007). MicroRNA-29 family reverts aberrant methylation in lung cancer by targeting DNA methyltransferases 3A and 3B. Proc. Natl. Acad. Sci. U. S. A. *104*, 15805–15810.

20. Benetti, R., Gonzalo, S., Jaco, I., Muñoz, P., Gonzalez, S., Schoeftner, S., Murchison, E., Andl, T., Chen, T., Klatt, P., et al. (2008). A mammalian microRNA cluster controls DNA methylation and telomere recombination via Rbl2-dependent regulation of DNA methyltransferases. Nat. Struct. Mol. Biol. *15*, 998.

21. Liu, L., van Groen, T., Kadish, I., and Tollefsbol, T.O. (2009). DNA methylation impacts on learning and memory in aging. Neurobiol. Aging *30*, 549–560.

22. Ciccarone, F., Tagliatesta, S., Caiafa, P., and Zampieri, M. (2018). DNA methylation dynamics in aging: how far are we from understanding the mechanisms? Mech. Ageing Dev. *174*, 3–17.

23. Gu, H., Smith, Z.D., Bock, C., Boyle, P., Gnirke, A., and Meissner, A. (2011). Preparation of reduced representation bisulfite sequencing libraries for genome-scale DNA methylation profiling. Nat. Protoc. *6*, 468–481.

24. Tognini, P., Napoli, D., Tola, J., Silingardi, D., Della Ragione, F., D'Esposito, M., and Pizzorusso, T. (2015). Experience-dependent DNA methylation regulates plasticity in the developing visual cortex. Nat. Neurosci. *18*, 956–958.

25. Miller, C.A., Gavin, C.F., White, J.A., Parrish, R.R., Honasoge, A., Yancey, C.R., Rivera, I.M., Rubio, M.D., Rumbaugh, G., and Sweatt, J.D. (2010). Cortical DNA methylation maintains remote memory. Nat. Neurosci. *13*, 664–666.

26. Lubin, F.D., Roth, T.L., and Sweatt, J.D. (2008). Epigenetic regulation of BDNF gene transcription in the consolidation of fear memory. J. Neurosci. *28*, 10576–10586.

27. Miller, C.A., and Sweatt, J.D. (2007). Covalent modification of DNA regulates memory formation. Neuron *53*, 857–869.

28. Lugli, G., Torvik, V.I., Larson, J., and Smalheiser, N.R. (2008). Expression of microRNAs and their precursors in synaptic fractions of adult mouse forebrain. J. Neurochem. *106*, 650–661.

29. Wang, W., Kwon, E.J., and Tsai, L.-H. (2012). MicroRNAs in learning, memory, and neurological diseases. Learn. Mem. *19*, 359–368.

30. Reh, R.K., Dias, B.G., Nelson, C.A., 3rd, Kaufer, D., Werker, J.F., Kolb, B., Levine, J.D., and Hensch, T.K. (2020). Critical period regulation across multiple timescales. Proc. Natl. Acad. Sci. U. S. A. *117*, 23242–23251.

31. Putignano, E., Lonetti, G., Cancedda, L., Ratto, G., Costa, M., Maffei, L., and Pizzorusso, T. (2007). Developmental downregulation of histone posttranslational modifications regulates visual cortical plasticity. Neuron *53*, 747–759.

32. Morita, S., Horii, T., Kimura, M., Ochiya, T., Tajima, S., and Hatada, I. (2013). miR-29 represses the activities of DNA methyltransferases and DNA demethylases. Int. J. Mol. Sci. *14*, 14647–14658.

33. Oliveira, A.M.M., Hemstedt, T.J., and Bading, H. (2012). Rescue of aging-associated decline in Dnmt3a2 expression restores cognitive abilities. Nat. Neurosci. *15*, 1111–1113.

34. Braasch, D.A., and Corey, D.R. (2001). Locked nucleic acid (LNA): fine-tuning the recognition of DNA and RNA. Chem. Biol. *8*, 1–7.

35. Smith, C.I.E., and Zain, R. (2019). Therapeutic Oligonucleotides: State of the Art. Annu. Rev. Pharmacol. Toxicol. *59*, 605–630.

36. Khvorova, A., and Watts, J.K. (2017). The chemical evolution of oligonucleotide therapies of clinical utility. Nat. Biotechnol. *35*, 238–248.

37. Bangasser, D.A., Waxler, D.E., Santollo, J., and Shors, T.J. (2006). Trace conditioning and the hippocampus: the importance of contiguity. J. Neurosci. *26*, 8702–8706.

38. Meissner, A., Gnirke, A., Bell, G.W., Ramsahoye, B., Lander, E.S., and Jaenisch, R. (2005). Reduced representation bisulfite sequencing for comparative high-resolution DNA methylation analysis. Nucleic Acids Res. *33*, 5868–5877.

39. Rattiner, L.M., Davis, M., French, C.T., and Ressler, K.J. (2004). Brain-derived neurotrophic factor and tyrosine kinase receptor B involvement in amygdala-dependent fear conditioning. J. Neurosci. *24*, 4796–4806.

40. Dias, B.G., Goodman, J.V., Ahluwalia, R., Easton, A.E., Andero, R., and Ressler, K.J. (2014). Amygdala-dependent fear memory consolidation via miR-34a and Notch signaling. Neuron *83*, 906–918.

41. Szklarczyk, D., Kirsch, R., Koutrouli, M., Nastou, K., Mehryary, F., Hachilif, R., Gable, A.L., Fang, T., Doncheva, N.T., Pyysalo, S., et al. (2023). The STRING database in 2023: protein-protein association networks and functional enrichment analyses for any sequenced genome of interest. Nucleic Acids Res. *51*, D638–D646.

42. Zhang, B., Gaiteri, C., Bodea, L.-G., Wang, Z., McElwee, J., Podtelezhnikov, A.A., Zhang, C., Xie, T., Tran, L., Dobrin, R., et al. (2013). Integrated systems approach identifies genetic nodes and networks in late-onset Alzheimer's disease. Cell *153*, 707–720.

43. Xin, W., Kaneko, M., Roth, R.H., Zhang, A., Nocera, S., Ding, J.B., Stryker, M.P., and Chan, J.R. (2024). Oligodendrocytes and myelin limit neuronal plasticity in visual cortex. Nature *633*, 856–863.

44. McGee, A.W., Yang, Y., Fischer, Q.S., Daw, N.W., and Strittmatter, S.M. (2005). Experience-driven plasticity of visual cortex limited by myelin and Nogo receptor. Science *309*, 2222–2226.

45. Wingo, T.S., Yang, J., Fan, W., Min Canon, S., Gerasimov, E.S., Lori, A., Logsdon, B., Yao, B., Seyfried, N.T., Lah, J.J., et al. (2020). Brain microRNAs associated with late-life depressive symptoms are also associated with cognitive trajectory and dementia. NPJ Genom Med *5*, 6.

46. Ugalde, A.P., Ramsay, A.J., de la Rosa, J., Varela, I., Mariño, G., Cadiñanos, J., Lu, J., Freije, J.M., and López-Otín, C. (2011). Aging and chronic DNA damage response activate a regulatory pathway involving miR-29 and p53. EMBO J. *30*, 2219–2232.

47. Barrett, R.M., and Wood, M.A. (2008). Beyond transcription factors: the role of chromatin modifying enzymes in regulating transcription required for memory. Learn. Mem. *15*, 460–467.

48. Oliveira, A.M.M., Hemstedt, T.J., Freitag, H.E., and Bading, H. (2016). Dnmt3a2: a hub for enhancing cognitive functions. Mol. Psychiatry *21*, 1130–1136.

49. Day, J.J., and Sweatt, J.D. (2010). DNA methylation and memory formation. Nat. Neurosci. *13*, 1319–1323.

50. Ferry, L., Fournier, A., Tsusaka, T., Adelmant, G., Shimazu, T., Matano, S., Kirsh, O., Amouroux, R., Dohmae, N., Suzuki, T., et al. (2017). Methylation of DNA Ligase 1 by G9a/GLP Recruits UHRF1 to Replicating DNA and Regulates DNA Methylation. Mol. Cell *67*, 550–565.e5.

51. Day, K., Waite, L.L., Thalacker-Mercer, A., West, A., Bamman, M.M., Brooks, J.D., Myers, R.M., and Absher, D. (2013). Differential DNA methylation with age displays both common and dynamic features across human tissues that are influenced by CpG landscape. Genome Biol. *14*, R102.

52. Jung, M., and Pfeifer, G.P. (2015). Aging and DNA methylation. BMC Biol. *13*, 7.

53. Oliveira, A.M.M. (2016). DNA methylation: a permissive mark in memory formation and maintenance. Learn. Mem. *23*, 587–593.

54. Gulmez Karaca, K., Kupke, J., Brito, D.V.C., Zeuch, B., Thome, C., Weichenhan, D., Lutsik, P., Plass, C., and Oliveira, A.M.M. (2020). Neuronal ensemble-specific DNA methylation strengthens engram stability. Nat. Commun. *11*, 639.

55. Guruharsha, K.G., Kankel, M.W., and Artavanis-Tsakonas, S. (2012). The Notch signalling system: recent insights into the complexity of a conserved pathway. Nat. Rev. Genet. *13*, 654–666.

56. Artavanis-Tsakonas, S., Rand, M.D., and Lake, R.J. (1999). Notch signaling: cell fate control and signal integration in development. Science *284*, 770–776.

57. Alberi, L., Hoey, S.E., Brai, E., Scotti, A.L., and Marathe, S. (2013). Notch signaling in the brain: in good and bad times. Ageing Res. Rev. *12*, 801–814.

58. Brai, E., Alina Raio, N., and Alberi, L. (2016). Notch1 hallmarks fibrillary depositions in

sporadic Alzheimer's disease. Acta Neuropathol Commun *4*, 64.

59. Yamada, K., Mizuno, M., and Nabeshima, T. (2002). Role for brain-derived neurotrophic factor in learning and memory. Life Sci. *70*, 735–744.

60. Tyler, W.J., Alonso, M., Bramham, C.R., and Pozzo-Miller, L.D. (2002). From acquisition to consolidation: on the role of brain-derived neurotrophic factor signaling in hippocampal-dependent learning. Learn. Mem. *9*, 224–237.

61. Minichiello, L., Korte, M., Wolfer, D., Kühn, R., Unsicker, K., Cestari, V., Rossi-Arnaud, C., Lipp, H.P., Bonhoeffer, T., and Klein, R. (1999). Essential role for TrkB receptors in hippocampus-mediated learning. Neuron *24*, 401–414.

62. Mu, J.S., Li, W.P., Yao, Z.B., and Zhou, X.F. (1999). Deprivation of endogenous brain-derived neurotrophic factor results in impairment of spatial learning and memory in adult rats. Brain Res. *835*, 259–265.

63. Alonso, M., Vianna, M.R.M., Depino, A.M., Mello e Souza, T., Pereira, P., Szapiro, G., Viola, H., Pitossi, F., Izquierdo, I., and Medina, J.H. (2002). BDNF-triggered events in the rat hippocampus are required for both short- and long-term memory formation. Hippocampus *12*, 551–560.

64. Jones, P.A. (1999). The DNA methylation paradox. Trends Genet. *15*, 34–37.

65. Jones, P.A. (2012). Functions of DNA methylation: islands, start sites, gene bodies and beyond. Nat. Rev. Genet. *13*, 484–492.

66. Steiner, D.F., Thomas, M.F., Hu, J.K., Yang, Z., Babiarz, J.E., Allen, C.D.C., Matloubian, M., Blelloch, R., and Ansel, K.M. (2011). MicroRNA-29 regulates T-box transcription factors and interferon-γ production in helper T cells. Immunity *35*, 169–181.

67. Liston, A., Papadopoulou, A.S., Danso-Abeam, D., and Dooley, J. (2012). MicroRNA-29 in the adaptive immune system: setting the threshold. Cell. Mol. Life Sci. *69*, 3533–3541.

68. Kluever, V., Russo, B., Mandad, S., Kumar, N.H., Alevra, M., Ori, A., Rizzoli, S.O., Urlaub, H., Schneider, A., and Fornasiero, E.F. (2022). Protein lifetimes in aged brains reveal a proteostatic adaptation linking physiological aging to neurodegeneration. Sci. Adv. *8*, eabn4437.

69. Smith, T., Heger, A., and Sudbery, I. (2017). UMI-tools: modeling sequencing errors in Unique Molecular Identifiers to improve quantification accuracy. Genome Res *27*, 491–499.

70. Bolger, A.M., Lohse, M., and Usadel, B. (2014). Trimmomatic: a flexible trimmer for Illumina sequence data. Bioinformatics *30*, 2114–2120.

71. Harrison, P.W., Amode, M.R., Austine-Orimoloye, O., Azov, A.G., Barba, M., Barnes, I., Becker, A., Bennett, R., Berry, A., Bhai, J., et al. (2024). Ensembl 2024. Nucleic Acids Res *52*, D891–D899.

72. Dobin, A., Davis, C.A., Schlesinger, F., Drenkow, J., Zaleski, C., Jha, S., Batut, P., Chaisson, M., and Gingeras, T.R. (2013). STAR: ultrafast universal RNA-seq aligner. Bioinformatics *29*, 15–21.

73. Li, H., Handsaker, B., Wysoker, A., Fennell, T., Ruan, J., Homer, N., Marth, G., Abecasis, G., Durbin, R., and 1000 Genome Project Data Processing Subgroup (2009).

The Sequence Alignment/Map format and SAMtools. Bioinformatics *25*, 2078–2079.

74. Smith, T., Heger, A., and Sudbery, I. (2017). UMI-tools: modeling sequencing errors in Unique Molecular Identifiers to improve quantification accuracy. Genome Res *27*, 491–499.

75. Liao, Y., Smyth, G.K., and Shi, W. (2014). featureCounts: an efficient general purpose program for assigning sequence reads to genomic features. Bioinformatics *30*, 923–930.

76. Harrison, P.W., Amode, M.R., Austine-Orimoloye, O., Azov, A.G., Barba, M., Barnes, I., Becker, A., Bennett, R., Berry, A., Bhai, J., et al. (2024). Ensembl 2024. Nucleic Acids Res. *52*, D891–D899.

77. Love, M.I., Huber, W., and Anders, S. (2014). Moderated estimation of fold change and dispersion for RNA-seq data with DESeq2. Genome Biol *15*, 550.